Check for updates

Recovery of uranium using epoxy-modified phosphorus pentasulfide as an efficient adsorbent for uranium extraction from aquatic environments

Magd M. Badr, [ID] [a] W. M. Youssef,*[b] Entesar M. Elgammal, [ID] *[b] A. E. M. Hussien[b] and M. H. Taha [ID] [b]

Epoxy-modified phosphorus pentasulfide (EPMPS) formulation was developed for the supported recovery of uranium from aquatic environments. The selected components of the prepared formulation were tailored to produce a rigid foamed polymeric material that was rich in phosphorus, nitrogen, sulfur and oxygen atoms, thus increasing chelating bonding possibilities with uranium. FT-IR and SEM were applied to physically characterize the resulting sorbent. At an equilibrium time of 30 min, the phase ratio S/L of 1 g L^{-1}, pH 3 and initial uranium concentration of 50 mg L^{-1} yielded an adsorption efficiency for uranium of 90%. An 85% elution of uranium from loaded EPMPS was achieved with 1 h shaking and a phase ratio (S/A) of 0.5 g/25 mL of 0.1 M CH$_3$COONa. Sorption isotherm designs were exploited to analyze the findings from the experiments. Uranium had an adsorption capability of about 78.7 mg g^{-1}. According to the results of uranium adsorption, when applied to an actual sample, EPMPS is a suitable substrate for uranium adsorption from nitrate media.

1. Introduction

Uranium is a heavy metal that is both chemically poisonous and radioactive. Since the leakage of radionuclides from Japan's Fukushima Daiichi nuclear power plant, uranium contamination has received considerable attention. Large amounts of uranium enter the environment through natural sources, and uranium mill tailings.[1,2] The WHO has defined a maximum contaminant value of 9 μg L^{-1} for U, whereas the US EPA has suggested the highest limit of 30 μg L^{-1} for U(vi) in drinking water.[3] Consequently, eliminating U from waste has become a serious and critical issue for the protection of the environment and human health.

During the last decade, research was focused on the production of polymeric materials, including certain electron donor groups. These electron donor groups, which contain phosphorous, sulfur, nitrogen, and/or oxygen, are distinguished by an increase in free electron pairs and negative charges on a material's surface and bulk. The presence of these functional groups and electron resonance can endow the created materials with certain novel features. The resulting materials will be beneficial in a variety of applications, such as metal extraction, catalysts, flame retardants, sensors,

supercapacitors, superconductors, semiconductors, batteries, and metal uptake.[4–19]

Various techniques have been implemented to remove uranium from liquid and radioactive solutions. The most often used procedures include chemical precipitation, ion exchange, liquid membrane, solvent extraction, and adsorption.[20,21] Adsorption has piqued the interest of researchers in recent decades owing to its efficacy and low cost in removing uranium and for allowing the recovery and reuse of metal ions from liquid solutions. Several materials have been investigated as adsorbents, including activated carbon,[22] zeolite, resin, olivine rock, coir pith, smectites, and kaolinite.[23–27]

In the present work, systems comprising epoxy (diglycidyl ether of bisphenol A-DGEBA) with phosphorus pentasulfide (PPS) and polyamines were developed, and their potential use in the sorption of uranium from aqueous solutions was investigated based on two factors: their chemical activity and porosity. Based on the chemical activity the surface of these blends contains free electrons forming partially negative charged polar functional groups of, phosphorus, sulfur, nitrogen, and oxygen.

In our research, we created a novel epoxy formulation comprising phosphorus, sulfur, nitrogen, and oxygen, with the aim of recovering uranium from nuclear industrial effluent through reacting the epoxy (diglycidyl ether of bisphenol A-DGEBA) with phosphorus pentasulfide (PPS) and polyamine. It was anticipated that the created formulation's higher phosphorus, nitrogen, sulfur, and oxygen contents would boost the possibility of reaction with the targeted heavy metal, in this study's case, uranium.
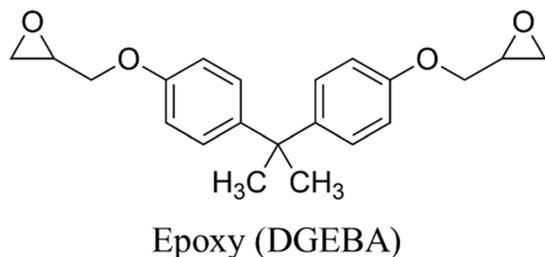
[a]Polymer Laboratory, Petrochemical Department, Egyptian Petroleum Research Institute, Nasr City, Cairo, 11727, Egypt. E-mail: themagd@yahoo.com; mmb@epri. sci.eg; Tel: +20 1002372636

[b]Nuclear Materials Authority, P.O. Box 530 Maadi, Cairo, Egypt. E-mail: entesarelgammal502@gmail.com; m.walid_nma@yahoo.com
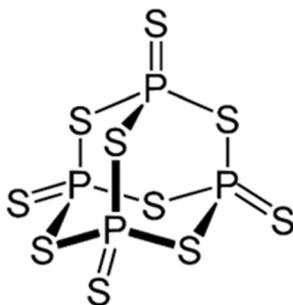
2.   Experimental

2.1.   Materials

Epoxy (DGEBA)

The epoxy was purchased from CMB Chemicals for Modern Building Company, Egypt under the trade name KEMAPOXY150 as an industrial two-pot epoxy, with vessel A containing the epoxy base, and vessel B the polyamine hardener.

Phosphorus pentasulfide (PPS)

Phosphorus pentasulfide (PPS) and acetone were provided by Adwic – El Nasr Pharmaceutical Co., Egypt. All the ingredients were used without any further purification.

2.2.   Epoxy-modified phosphorus pentasulfide (EPMPS) sample preparation and film formation

First, 10 mL of epoxy base (pot A) was dissolved in 10 mL of acetone (solvent), and the resulting mixture was agitated for 10 min at room temperature in a two-necked round-bottomed flask with a magnetic stirrer and reflux condenser. Next, 10 mL of ethylene glycol (EG) was used to dissolve 5 g of PPS,

which was then added dropwise to the main solution and agitated for an additional 30 min at room temperature. To the main solution, 10 mL of polyamine hardener (pot B) was added while continuously shaking for 3 min at room temperature. The solution was then sonicated for 3 min. The prepared material was then baked for 12 h at 80 °C to cure it. Before utilizing or performing any measurements, the material was left to stand at room temperature for 24 h (Fig. 1).

2.3.   Material characterization

The structural properties of the EPMPS were investigated using Fourier transform infrared spectrometry (FT-IR), scanning electron microscopy (SEM), and EDX. A Thermo-Scientific Nicolet IS10 instrument model (Germany) was used for the FT-IR analysis. The SEM equipment utilized was a Philips XL 30 ESEM (25–30 keV accelerating voltage, 1–2 mm beam diameter, and 60–120 s counting time), which was also linked to an EDX unit. The minimum detectable weight concentration ranged from 0.1–1 wt%, and the instrument realized a precision of less than 1%.

2.4.   Preparation of the metal solutions

All the reagents utilized were of analytical grade. The uranium stock solution contained 1000 mg L^{-1} uranium. The Arsenazo III complex technique was used to assay the uranium in its various working aqueous phases.[28] A Lambada UV/vis spectrophotometer (PerkinElmer, USA) was used to evaluate the absorbance of the produced uranium Arsenazo III complex at 650 nm in comparison with appropriate standard solutions.

2.5.   Batch experiments for the adsorption and elution studies

The adsorption process was controlled by a number of variables that were investigated. The solution pH, contact time, initial uranium concentration, and solid/liquid ratio were among these variables. In a typical experiment for the adsorption studies, 0.1 g of EPMPS was shaken with 100 mL uranium solution (50–600 mg L^{-1}) in a pH range of 0.5–5. The effect of Co ions was investigated. The flasks were sealed and set on a mechanical shaker at various temperatures (ranging from 25 °C to 50 °C). All the experiments were carried out triplicate, and

Fig. 1   Photographs of the cured created polymeric material of epoxy-modified phosphorus pentasulfide (EPMPS) formulation, and the material after grinding.

Table 1 Parameters for testing the different types of epoxy for the adsorption of uranium ions from aqueous solution

Type	pH	Time (min)	S/L ratio (g L^{-1})	Temp.	q_e (mg g^{-1})
Epoxy only (not modified)	3	30	1.0	Room temperature	26
EPMPS	3	30	1.0	Room temperature	78.7

mean values of 4% relative errors were used. The filtrate's uranium content was examined. The amount of adsorbed uranium (q_e) was estimated *via* eqn (1) by dividing the difference between the initial and residual amounts of uranium in solution by the mass of the adsorbent. The system's removal or adsorption efficiency (R_e), calculated using eqn (2), was expressed as the UO$_2^{2+}$ removal percentage in relation to the initial concentration. For uranium elution from the loaded EPMPS, a number of eluting agents were tested, namely HCl, H$_2$SO$_4$, Na$_2$CO$_3$, HNO$_3$, and NaCl.

$$q_e = \frac{C_o - C_e}{M} \times V \quad (1)$$

$$R_e = \frac{C_o - C_e}{C_o} \times 100 \quad (2)$$

where q_e (mg g^{-1}) is the amount of uranium adsorbed per unit mass of adsorbent, C_o and C_e are the initial and equilibrium (or at any time) ion concentration (mg L^{-1}), respectively, V is the volume in liters of solution, and M is the mass (g) of the EPMPS.

Table 1 shows that the effectiveness of the various types of prepared epoxy against uranium varied significantly. It was discovered that the epoxy modified by phosphorus pentasulfide was the best for uranium sorption because of the unique phosphorus-, sulfur-, nitrogen-, and oxygen-containing epoxy formulation created by reacting epoxy with phosphorus pentasulfide (PPS).

2.6. Liquid waste properties

The liquid waste solution was supplied from uranium ore processing in Anshas, Egypt. The main chemical composition comprised UO$_2^{2+}$, Fe^{3+}, and Ca^{2+} at concentrations of 80 mg L^{-1}, 1.6 g L^{-1}, and 1 g L^{-1}, respectively.

3. Results and discussion

3.1. Characterization

3.1.1. FT-IR spectral study. It was anticipated that the polarized atoms of phosphorus, sulfur, nitrogen, and oxygen in the composition of the reactant ingredients would result in a prepared polymeric material with a variety of functional groups and bonding kinds. Fig. 2 records and compiles the FT-IR spectra as well as the spectral data of the synthesized EPMPS both before and after uranium adsorption. In the spectra, the stretching of the aromatic rings' C=C and C–C bonds were indicated by the peaks at 1608 and 1509 cm^{-1}, while stretching of the C–O–C bonds corresponding to the ether linkage was shown at 1000–1100 cm^{-1}. The oxirane group's C–O distortion was the reason for the peak's absence at 915 cm^{-1}, which indicated that all of the epoxy rings were consumed through the reactions during the treatment process. Within the range of 2900–3700 cm^{-1}, the bands of amine groups and hydroxyl groups' hydrogen bonds overlapped each other. In the primary amines, N–H deformation was observed at 1650–1500 cm^{-1}; while in the secondary amines, this was shifted toward lower
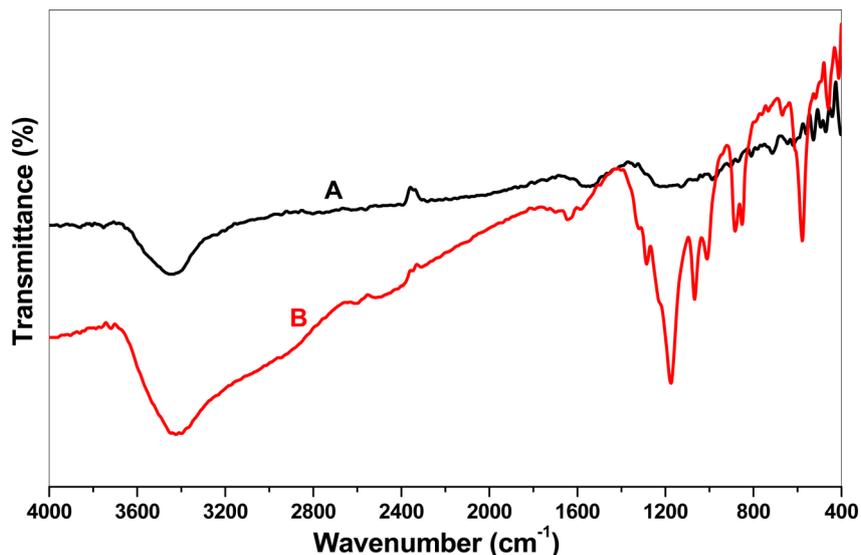

Fig. 2 FT-IR spectra of EPMPS (A) before and (B) after uranium adsorption.

wavenumbers (1580–1490 cm^{-1}) and was typically weak. Strongly coupled to the C–N band, C=S stretching yielded a band at 1230–1030 cm^{-1}. The P=S's stretching vibration band displayed a medium intensity and was located at 758.88 cm^{-1}. There was also a variable intensity band at 552.53 cm^{-1}, which may have been caused by the stretching vibration of the P–S bond, which may have been shifted to a higher frequency due to the nearby highly electronegative groups and atoms. The asymmetric stretching vibrations of the aliphatic methoxy P–O–C group were observed by very strong broad bands of pentavalent and trivalent methoxy compounds at 1063.56 and 1026.95 cm^{-1}, respectively, as well as a characteristic symmetric methyl deformation band at 1363.48 cm^{-1}.

At 945.95 cm^{-1}, pentavalent ethoxy compounds showed a further strong band. Compounds containing methoxy and ethoxy had a prominent band at 827.35 cm^{-1}, which was most likely caused by the P–O–C group stretching symmetrically. The P–O–C methoxy group was responsible for a sharp band at 1182.20 cm^{-1}. The band observed at 995–855 cm^{-1} resulted from the P–O–C asymmetric stretching vibration for aromatic compounds, specifically P–O–phenyl, which was coupled with a strong band at 945.95 cm^{-1}. In the vicinity of 758.88 cm^{-1}, the P–C bond's stretching vibration produced a medium-to-strong band. A medium-to-strong intensity band was also present in the phenyl–P bond because of an aromatic ring vibration at 1457.09 cm^{-1}. The P=O group's stretching vibration strong band lay between 1350 and 1150 cm^{-1}. It is possible that all of the phosphorus atoms were occupied with other types of bonding, which is why there was no sharp band for P–H group stretching vibration observed in the region of 2265–2285 cm^{-1} and no weak-to-medium intensity broad bands of the P–O–H group for its O–H stretching vibration at 2100–2300 cm^{-1} or its hydrogen bonding at 2560–2700 cm^{-1}.[29-33]

The FT-IR spectra of EPMPS both before and after uranium adsorption are shown in Fig. 2. Fig. 2A provides for a qualitative assessment of the functional groups linked to the EPMPS modified phosphorus pentasulfide through using the FT-IR spectra. Fig. 2B unequivocally demonstrates the presence of multiple peaks in both scenarios, including a peak at approximately 3600 cm^{-1} that was linked to O–H stretching. Alkene C=C bending bands were observed at 977 and 888 cm^{-1}, while bending N–H bands were found at 3398 and 1380 cm^{-1} and further connected to vinyl group C–N stretching bands at 1117 cm^{-1}. In the modified material, the C–H bad was stretched at 704–616 cm^{-1} and at 1200 cm^{-1} related to uranium adsorption.

3.1.2. SEM/EDX analysis studies. Fig. 3A and B illustrate the results from the SEM/EDX analysis used to examine the surface morphology and elemental composition of EPMPS before and after uranium adsorption, respectively. Fig. 3A shows the formation of pores and crevices on the EPMPS surface, which may have occurred as a result of the volatility and decomposition of the low molecular weight compounds during the synthesis process and thermal treatment. These pores and cracks were filled with uranium ions following adsorption (Fig. 3B). The EDX plot in Fig. 3A revealed the presence of P, S,
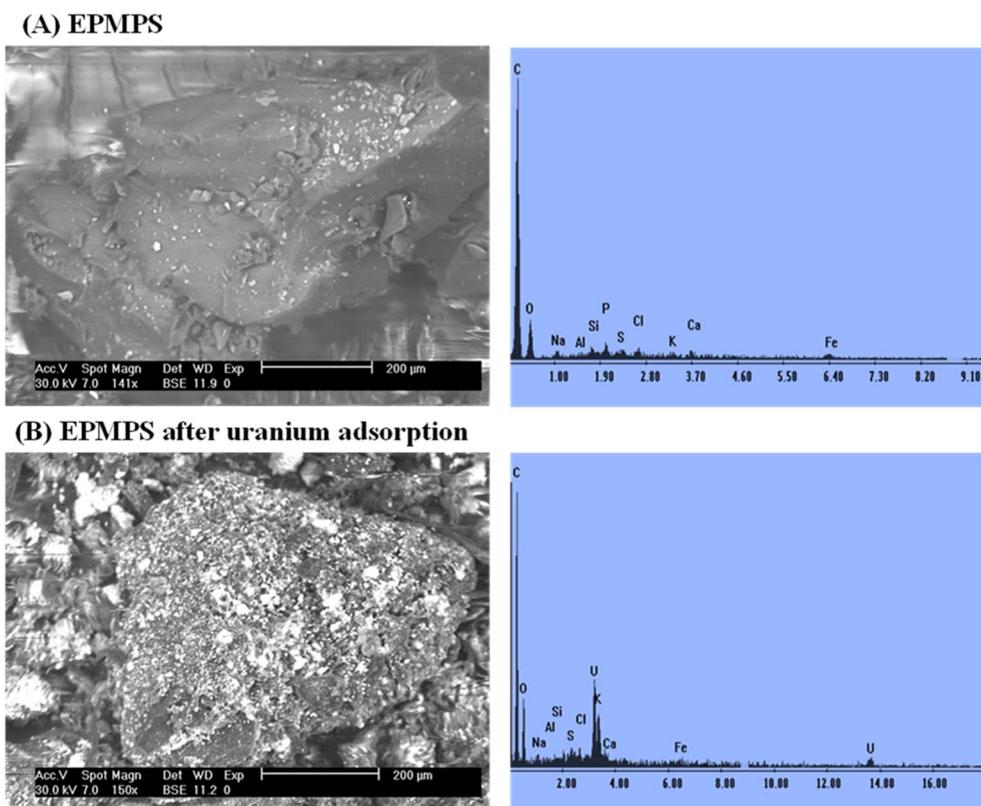

Fig. 3 SEM images and EDX spectra of EPMPS (A) before and (B) after uranium adsorption.

and O in the EPMPS, while the N peak was obscured by the plot's packed area. The presence of U on the EPMPS/U was verified by the EDX plot in Fig. 3B, confirming the successful uranium adsorption process when utilizing the EPMPS polymeric material.

The other elements detected by EDX could be attributed to the presence of impurities in the commercial material or the high activity of the functional groups of the reactants, whereby the synthesized EPMPS reacted with materials on the surface of the glassy container during the reaction process, which may have caused other elements to emerge in the EDX plots.

3.2. Parameters influencing the adsorption procedures

3.2.1. Impact of pH. Fig. 4A illustrates how the pH affects the sorption of metal ions (U(VI)) using EPMPS. In the tests, the temperature, solution volume, sorbent dosage, shaking time, and initial metal ion concentration were all fixed at the same values to assess the pH effect, *i.e.*, 25 °C, 1.0 g L^{-1}, 120 min, and 50 mg L^{-1} uranium concentration, respectively. We examined the pH effects by varying the pH in the range of pH 0.5–5.0. A key operational variable in the adsorption procedure is the pH of the working solution as this can affect the level of adsorbent ionization throughout the reaction, dissolution of the uranium

ions, and the amount of opposing ions on the functional groupings of the adsorbent being utilized.[34] Fig. 4A shows that as the pH levels was increased, so did the removal percentage of metal ions (R_e). The biggest increase in uranium adsorption with EPMPS was from 18% to 90%, while at pH levels greater than 3, uranium adsorption fell to 66% at pH 5.[27]

3.2.2. Impact of time. The changes in the metal elimination percentage over time using EPMPS are shown in Fig. 4B. In the experiments, 1.0 g L^{-1} of EPMPS was added to an aqueous solution of 50 mg L^{-1} U(VI) at pH 3, with varying the shaking time from 5–120 min. The uranium adsorption efficiency rose from 68% to 90% as the shaking time was increased from 5.0 to 30.0 min, while further increasing the shaking time had only a slightly impact on the adsorption efficiency. Therefore, 30 min contact period was chosen as an appropriate shaking time.

3.2.3. Impact of adsorbent dosage. A number of batch experiments were performed with varying the adsorbent amount as 0.01, 0.05, 0.1, 0.12, 0.15, and 0.2 g/100 mL of test solution at pH 3 in order to optimize the treatment system. According to Fig. 4C, raising the dosage of the adsorbent from 0.01 g (nearly 50%) to 0.1 g (nearly 90%) increased the adsorption effectiveness, while more than 0.1 g of adsorbent raised the uranium adsorption efficiency to 91.8% at 0.2 g/100
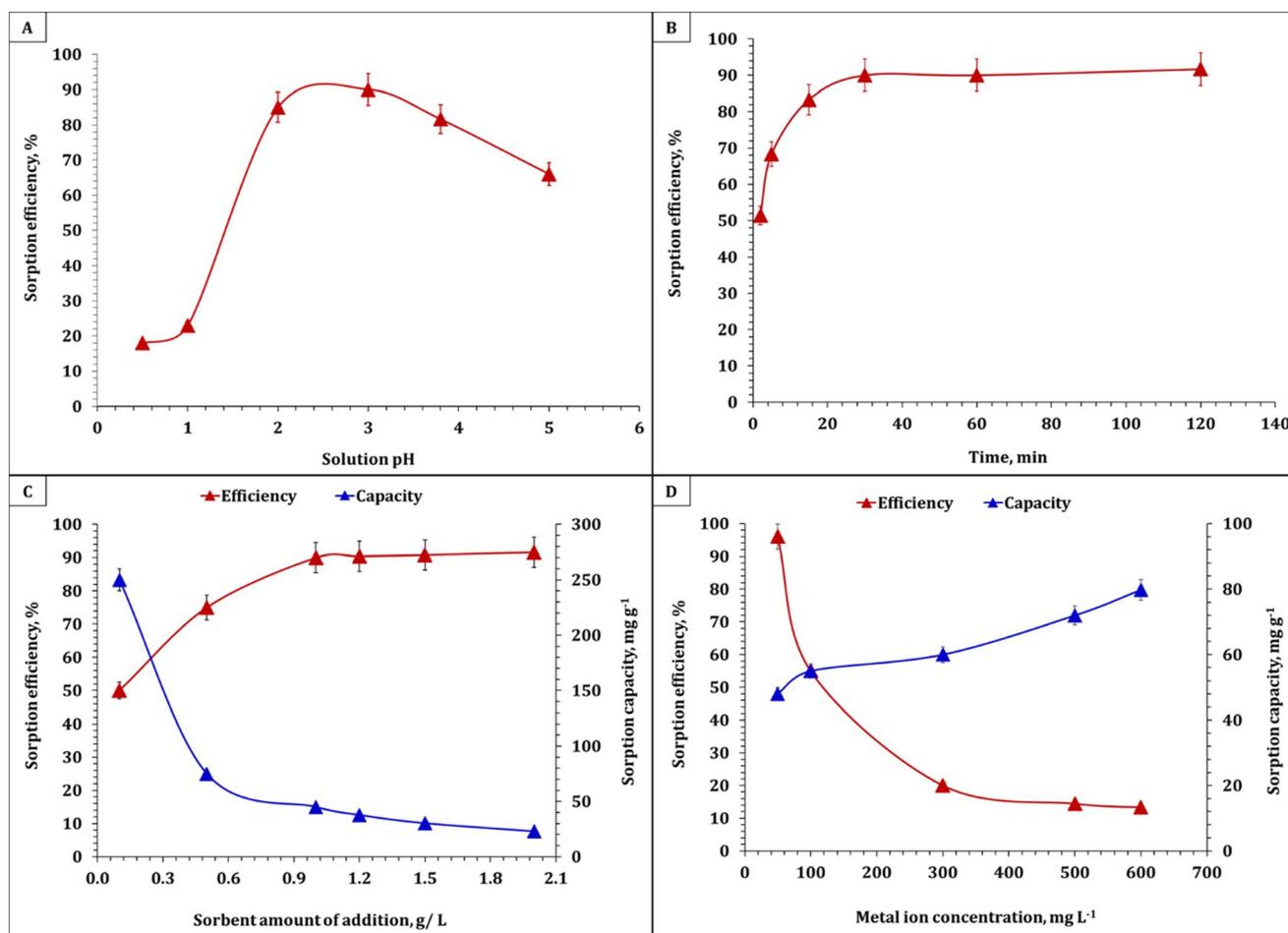

Fig. 4 Impact of (A) pH, (B) time, (C) adsorbent dosage, and (D) original uranium content on the uranium adsorption efficiency on EPMPS.

mL, showing only a minor increase. It is worth noting that the uranium adsorption capacity decreased from 250 to 37.6 mg g^{-1} as the sorbent dose was increased from 0.01 to 0.1 g. Therefore, from an economic standpoint, a 0.1 g dose was selected as optimal.

3.2.4. Impact of the preliminary uranium concentration. A predetermined weight 1.0 g L^{-1} was used to conduct a variety of tests at various uranium concentrations at 25 °C and pH 3. This was done in order to clarify how the concentration of uranium affects the efficiency of adsorption on EPMPS. At 30 min, the preliminary uranium contents under study were varied from 50 to 600 mg L^{-1}. The acquired findings are presented in Fig. 4D, and show that when the initial uranium concentration was increased, the uranium removal efficiency declined. This may

have occurred as a result of the greater mobility of uranyl ions (UO$_2^{2+}$) in the diluted solutions, which heightens the ion–adsorbent interactions.[35] In addition, the sorption capacity rose from 48.0 to 79.8 mg g^{-1} as the initial concentration was boosted from 50 to 600 mg L^{-1}. The highest uranium removal was seen at 50 mg L^{-1} uranium concentration.

3.3. Kinetic modeling

The current study used three equations from various adsorption kinetic models, as listed in Table 2.[36]

The previously described kinetic models for uranium adsorption on EPMPS are presented in Fig. 5A–C and Table 3 lists their kinetic parameters.

The PS kinetic model, which had higher R^2 coefficients than the LPF model, was found to be the most precise in matching the experimental results. Additionally, Table 3 illustrates how well the measured adsorption capacity and the theoretical adsorption capacity of the composite at equilibrium matched. These results suggest that the technique of sorption is dependent on the quantity of ions and follows the PS kinetic model.[37] Additionally, it was shown that the rate-controlling step involved electron transfer between the UO$_2^{2+}$ ions and the material's functional groups during chemical sorption.[38] These

Table 2 Adsorption kinetic models used and their equations

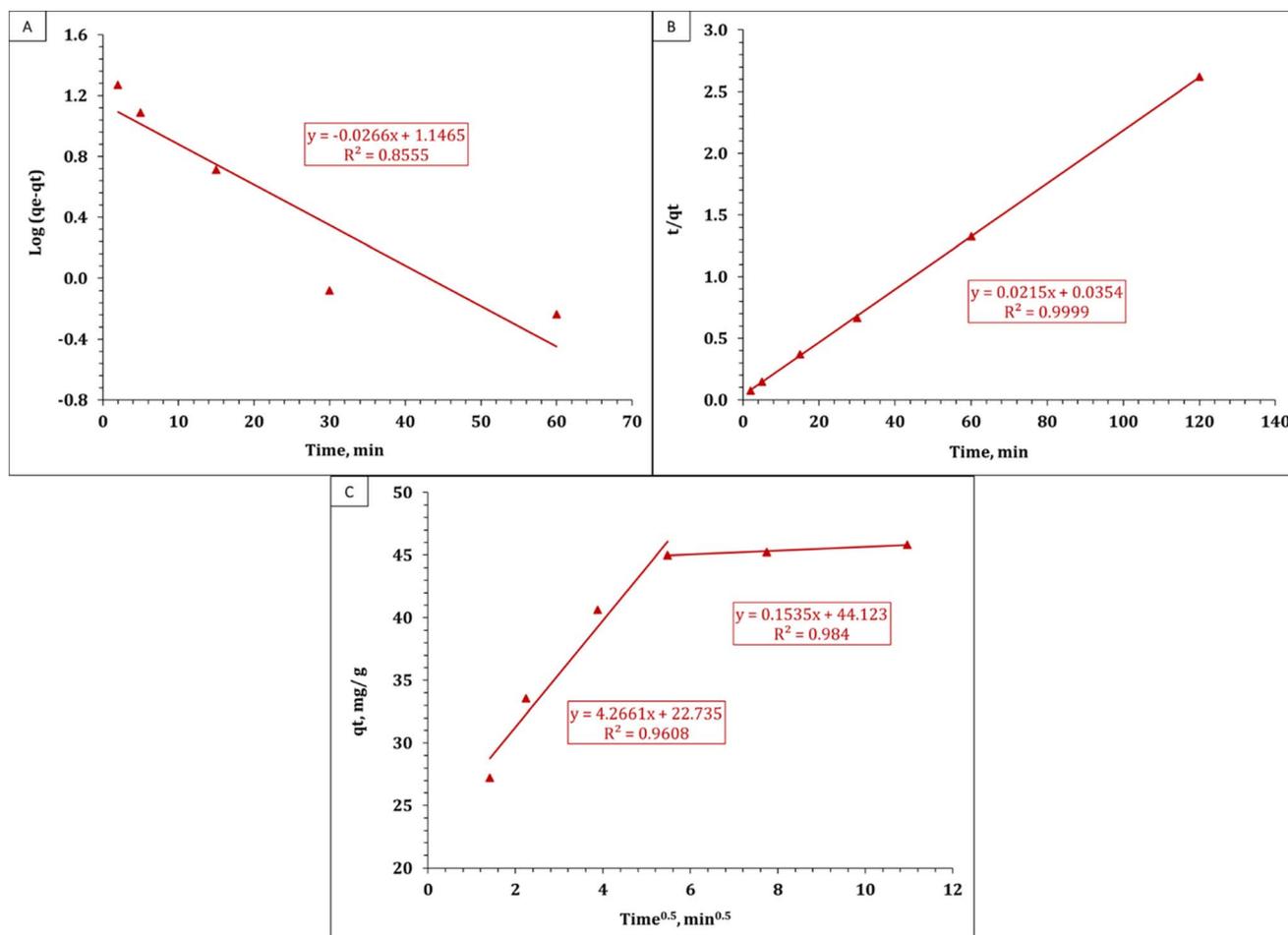| Adsorption kinetic models	Equations
Lagergren pseudo-first-order (LPF) model	$\log(q_e - q_t) = \log q_e - (K_1/2.303)t$ (3)
Pseudo-second-order (PS) model	$t/q_t = 1/K_2 q_e^2 + (1/q_e)t$ (4)
Weber and Morris (W&M) model	$q_t = K_{id}t^{0.5} + C$ (5)

Fig. 5 The three adsorption kinetic models of uranium adsorption upon EPMPS.

Table 3 Computed parameters of the various kinetic adsorption models used

Lagergren pseudo-first-order model	k_1 (min^{-1})	0.061
	$q_{e,cal}$ (mg g^{-1})	14.0
	$q_{e,exp}$ (mg g^{-1})	45.8
	R^2	0.85
Pseudo-second-order model	k_2 (min^{-1})	0.013
	$q_{e,cal}$ (mg g^{-1})	46.5
	$q_{e,exp}$ (mg g^{-1})	45.8
	h (mol g^{-1} h^{-1})	28.25
	$t_{1/2}$ (h)	1.6
	R^2	0.99
Weber and Morris model	Stage I	
	k_i (mg g^{-1} min$^{-1/2}$)	4.27
	C	22.7
	R^2	0.96
	Stage II	
	k_i (mg g^{-1} min$^{-1/2}$)	0.15
	C	44.1
	R^2	0.98

results highlight the usefulness of the PS kinetic model in assessing the adsorption operation and shed light on the mechanisms governing uranium pickup by the adsorbent.

3.4. Adsorption isotherms

A number of frequently used adsorption isotherm models were considered in order to match the reported isotherm models under the equilibrium adsorption of EPMPS. These models included the Freundlich, Langmuir, and Temkin isotherms, whose equations[39–41] are shown in Table 4.

A straight line with an intercept of ($\log K_F$) and a slope of ($1/n$) could be seen in Fig. 6A. The Freundlich, Langmuir, and Temkin isotherms are displayed in Table 5. The straight line with a slope of ($1/Q_o$) and an intercept of $1/bQ_o$ is shown in Fig. 6B. Using the Langmuir parameters given in Table 4, one may use the dimensionless separation factor R_L in eqn (9) listed in Table 4 to predict the affinity between the sorbate and sorbent. The results from the Timken model are illustrated in Fig. 6D. The R_L value, which can be either irreversible ($R_L = 0$), favorable ($0 < R_L < 1$), or unfavorable ($R_L > 1$), determines the type of isotherm. According to Fig. 6C, the dimensionless separation factor values for uranium(VI) adsorption onto EPMPS reveal that greater initial uranium(VI) concentrations were preferred over lower concentrations for uranium(VI) adsorption. Table 5 illustrates the data after applying the equations for the isotherms, namely the Freundlich, Langmuir, and Timken parameters for uranium adsorption onto EPMPS.

Table 4 Models of adsorption isotherms and their formulas

Adsorption isotherms	Equations
Freundlich isotherm	$q_e = K_f C_e^{1/n}$ (6)
	$\log q_e = \log K_f + (1/n) \log C_e$ (7)
Langmuir isotherm	$C_e/q_e = 1/bQ_o + C_e/Q_o$ (8)
	$R_L = 1/(1 + bC_o)$ (9)
Temkin isotherm	$Q_e = B \ln AT + B \ln C_e$ (10)

The results of the experiments demonstrated that uranium adsorption on EPMPS more closely matched the Langmuir isotherm than the Freundlich and Temkin isotherms.

Table 6 provides a comparison of the EPMPS adsorption capability with different sorbents.

3.5. Impact of temperature

The influence of temperature on the uranium removal efficiency was studied at temperatures ranging from 25 °C to 50 °C for 30 min and 0.1 g EPMPS/100 mL solution. Fig. 7A depicts the resulting removal efficiencies, which reveal that temperature did not play a critical role in the removal of uranium. After reaching room temperature, the efficiency of uranium removal did not continue to increase; rather, it decreased as the temperature rose. The diminishing effect of the surface activity, which would result in a thinner boundary layer at higher temperatures due to U(VI)'s increased tendency to escape into the solution, may be the cause of the decrease in uranium absorption capacity with the increase in temperature.

3.6. Adsorption thermodynamics

The thermodynamic properties of the adsorption procedure were ascertained through experiments conducted at different temperatures. The mathematical equations shown in Table 7 were used to calculate the system's thermodynamic features and Gibbs free energy ($\Delta G°$).[46,47] Fig. 7B shows both the enthalpy ($\Delta H°$) and entropy ($\Delta S°$) values derived from the $\log K_C$ vs. $1/T$ plots using a curve-fitting tool. Also Table 8 provides the thermodynamic parameter values for uranium ion sorption onto EPMPS.

The results show that $\Delta H°$ possessed negative values and that uranium sorption onto EPMPS was is exothermic. Moreover, $\Delta G°$ exhibited negative values across the range of sorption temperatures, suggesting that the sorption process appeared to be feasible as well as spontaneous. A negative value of $\Delta S°$ indicates a reduction in the disorder of the solid–aqueous interface.[48,49]

3.7. Effect of opposite ions

The influence of other metal ions, such as cadmium, copper, thorium, calcium, and iron, which may be present simultaneously with uranium ions in the aqueous solution, was investigated by adding different cations at a concentration 100 ppm, individually to the solution containing uranium under the optimal conditions. As opposing ions were introduced, the percentage of uranium uptake on EPMPS decreased, as shown in Fig. 8. Consequently, we were able to identify the alterations and deleterious consequences that impact uranium's absorption in comparison to competing ions.

3.8. Metal desorption

We examined metal elution from different solutions of the loaded EPMPS, namely CH$_3$COONa, HNO$_3$, HCl, acetic acid, and NaCl. The loaded EPMPS polymeric material (0.5 g) was shaken with the eluent parts (25 mL) in order to conduct the elution
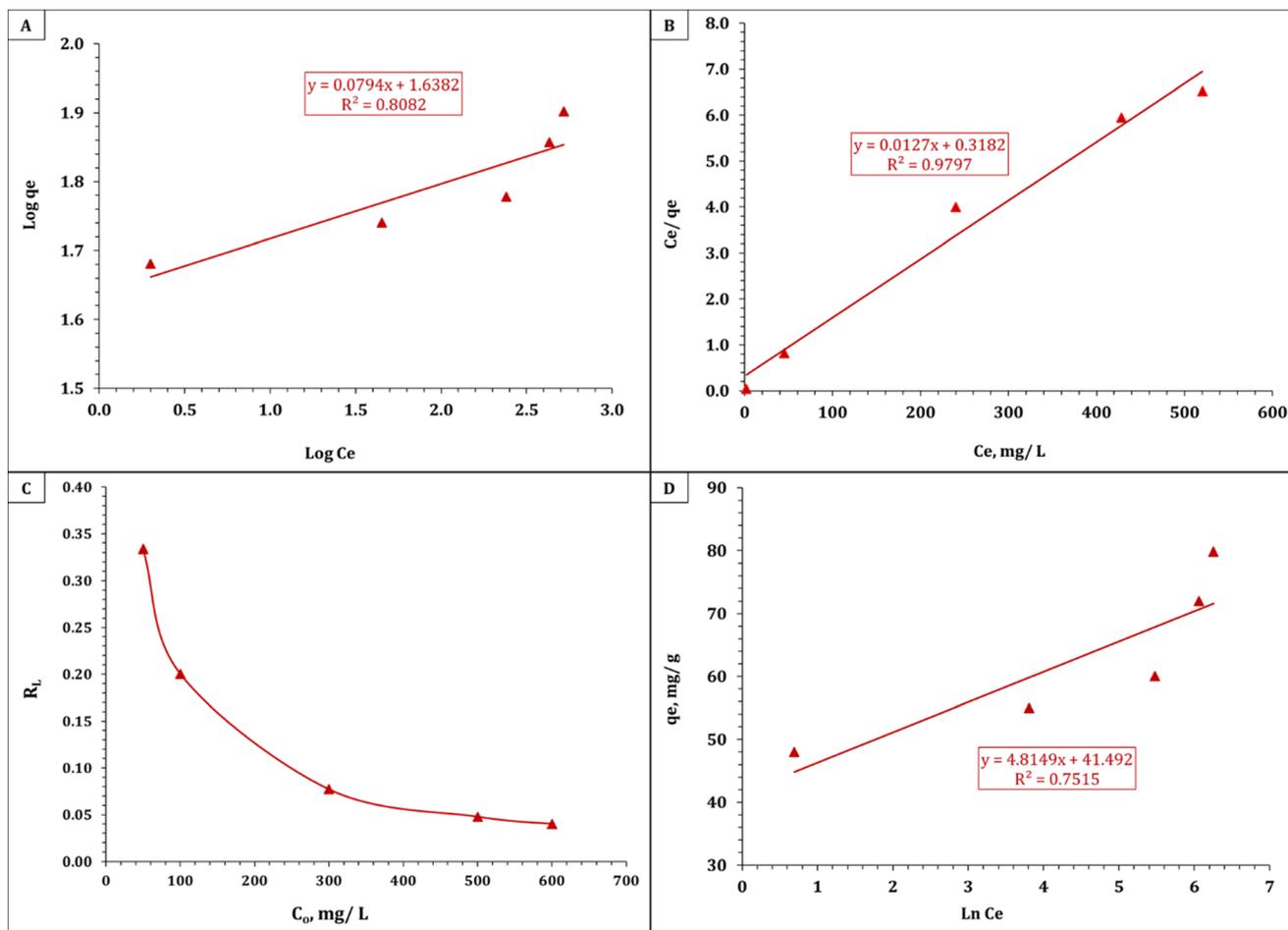
Fig. 6 (A) Freundlich isotherm plot, (B) Langmuir isotherm plot, (C) separation factor R_L, and (D) Temkin isotherm plot for the adsorption of uranium on EPMPS.

Table 5 Langmuir, Freundlich, and Temkin parameters for uranium adsorption on EPMPS

Freundlich isotherm model	n	12.59
	K_f (mg g^{-1})	43.47
	R^2	0.80
Langmuir isotherm model	Q_m (mg g^{-1})	78.74
	b (L mg^{-1})	0.040
	R^2	0.98
Temkin isotherm	b (J mol^{-1})	514.56
	B	4.8
	K_T (L g^{-1})	5527.1
	R^2	0.75

studies. The amount of eluted metal was calculated following analysis of the metal in the collected samples. Fig. 9 provides a summary of the findings, and it is evident that the CH$_3$-COONa[50] elution solution was the most effective eluent for obtaining uranium loaded on the EPMPS.

3.9. Adsorption mechanism of uranium on the prepared adsorbent

In the current study, uranium sorption from aqueous solution was investigated utilizing EPMPS. Understanding the sorption

mechanism was necessary to comprehend the sorption process and to create an efficient flow sheet for uranium recovery from aqueous solution using EPMPS, as a viable substitute for the traditional liquid–liquid technique. To the best of our knowledge, there has not yet been any research done on the mechanism of uranium sorption from aqueous solution using EPMPS. The physicochemical traits of EPMPS's functional groups are

Table 6 Epoxy and EPMPS experimental capacities in comparison to a few other sorbents' sorption capacities

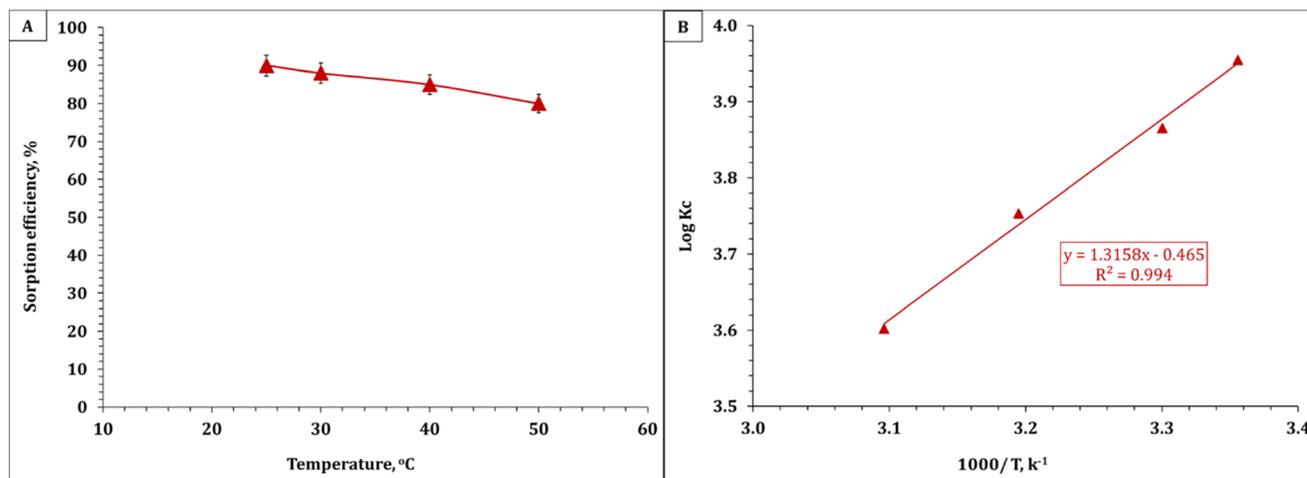| Type/reference	Sorption capacity (mg g^{-1})
Acrylic and diaminomaleonitrile-modified cellulose[42]	328.95
Amidoxime-functionalized flower-like Fe$_3$O$_4$@TiO$_2$ core–shell microspheres[43]	313.6
Rice steam[44]	11.36
Metal–organic frameworks and covalent–organic frameworks[45]	2.68
Epoxy	26
EPMPS	78.7

Fig. 7 (A) Effect of temperature on the percentage removal of uranium with EPMPS at pH 3 in 30 min. (B) Van't Hoff equation plot for uranium sorption.

Table 7 Adsorption thermodynamics investigated and their equations

Adsorption thermodynamics	Equations
Thermodynamic parameters calculation	$\log K_C = -\dfrac{\Delta H^\circ}{2.303R} \times \dfrac{1}{T} + C$ (11)
Gibbs free energy (ΔG°)	$-\Delta G^\circ = 2.303RT \log K_C$ (12)
	$\Delta G^\circ = \Delta H^\circ - T\Delta S^\circ$ (13)

Table 8 Thermodynamic parameters for uranium adsorption on EPMPS

ΔG (kJ mol^{-1})				ΔH (kJ mol^{-1})	ΔS (J mol^{-1} K^{-1})
25 °C	30 °C	40 °C	50 °C		
−22.56	−22.42	−22.49	−22.28	−25.19	−8.83

mostly responsible for its solid liquid properties. Fig. 10 presents a proposed adsorption mechanism (through chemical interactions and the porosity of the material) of uranium onto EPMPS. Phosphorus, sulfur, nitrogen, and oxygen were necessary for the partially negative charged polar functional from free
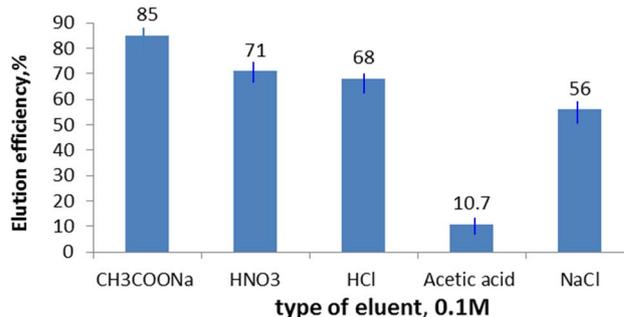

Fig. 9 Effect of the eluent type on uranium elution efficiency.
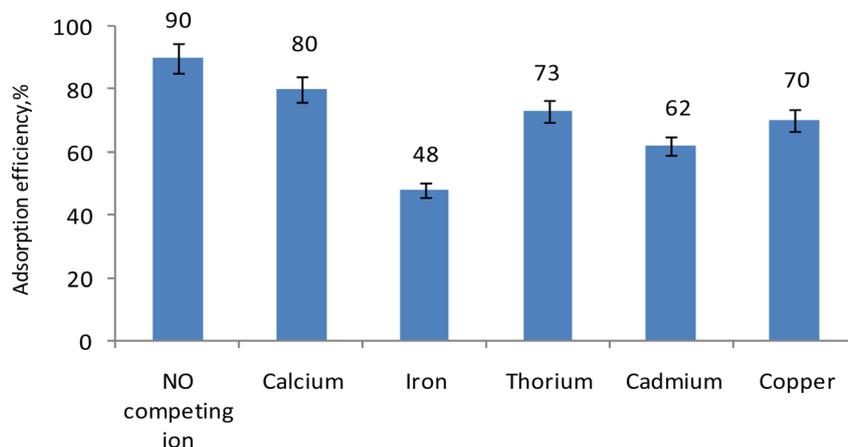

Fig. 8 Effect of some competing ions on the efficiency of the adsorbed uranium, showing adsorption efficiency (%) from its solution by EPMPS at pH 3 in 30 min.
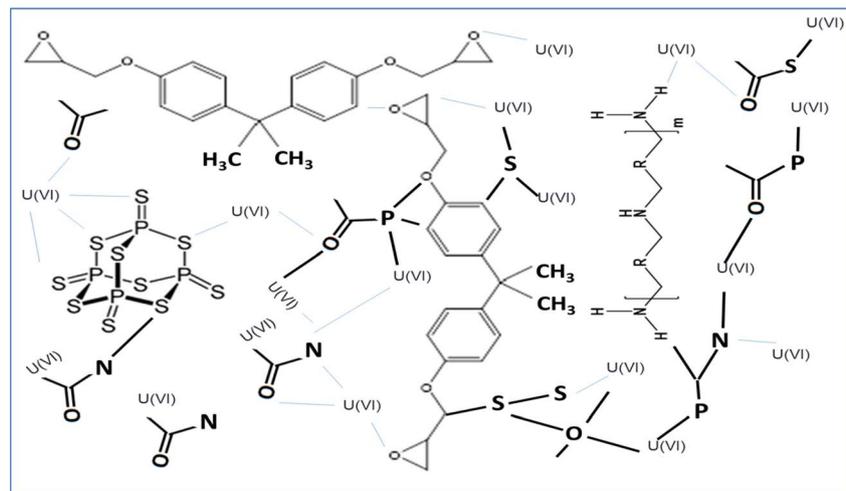
Fig. 10 Proposed chemical mechanism of uranium adsorption on the synthesized epoxy.

Table 9 Chemical composition of the applied waste solution

Element	Concentration ($mg\ L^{-1}$)
Cl	16
Fe	1600
UO_2	80
Cu	2
SiO_2	800
SO_4^{2}	53
CO_3^{2}	80
Mn	230

electron that contained surface EPMPS, hydroxyl, amines, ether, and raw epoxy. The physical mechanism followed thermal curing, as the curative procedure by heat caused openings inside the EPMPS as it is a spongy material. These two variables were obviously necessary for the synthesized EPMPS material.

3.10. Case study

Application of the sorption results was performed, wherein 10 mL of waste solution (from an ore processing unit (Project 8, Inshass, NMA, Egypt))[46] containing 80 mg L^{-1} of uranium (Table 9) was contacted with 0.1 g of EPMPS for 30 min at room temperature (25 ± 2) °C and at pH 3. After the solution had equilibrated, its uranium content was assessed, and it was found that the overall sorption capacity of EPMPS was 82% and 75% of the adsorbed uranium was desorbed by 0.1 M CH₃-COONa (70%).

4. Conclusion

This study investigated the use of EPMPS to adsorb uranium from aqueous solution. The results show that several factors, comprising the pH, time, adsorbent amount, initial uranium content, temperature, and opposite ions, significantly influenced the removal of uranium by adsorption on to EPMPS. The adsorption process was found to rise with increasing the

shaking duration and the adsorbent weight and decreased with the rising temperature and metal concentration. The experimental data best followed the Langmuir model. It was confirmed by this study that a novel material was synthesized with novel properties, which is suitable for uranium sorption and is highly recommended for some other applications, including metal extraction and catalysts. Our next task will be to create the material at the nanoscale and with several additional chemical compositions and to further test its utility.

Abbreviations

EPMPS	Epoxy-modified phosphorus pentasulfide
DGEBA	Diglycidyl ether of bisphenol A
LPF	Lagergren pseudo-first-order
PS	Pseudo-second-order
W&M	Weber and Morris

Data availability

The data supporting this article have been included in this manuscript.

Conflicts of interest

There are no conflicts to declare.

References

1 L. M. Camacho, S. Deng and R. R. Parra, *J. Hazard. Mater.*, 2010, **175**, 393–398.
2 H. Parab, S. Joshi, N. R. Shenoy, V. A. Lali and M. Sudersanan, *Bioresour. Technol.*, 2005, **96**, 1241–1248.

3 F. Ma, Y. Gui, P. Liu, Y. Xue and W. Song, *J. Chem. Eng.*, 2020, **390**, 124597, DOI: 10.1016/j.cej.2020.124597.

4 X. Zhou and T. Wu, *Chemosphere*, 2019, **235**, 163–168.

5 F. A. Ibrahim and M. B. Magd, *Front. Sci. Res. Technol.*, 2023, **5**, 41–51.

6 D. K. Kakati and M. H. George, *Polymer*, 1993, **34**, 4319–4324.

7 S. Iliescu, L. Zubizarreta, N. Plesu, L. Macarie, A. Popa and G. Ilia, *Chem. Cent. J.*, 2012, **6**, 1–13.

8 S. Monge and G. David, *Phosphorus-based Polymers: from Synthesis to Applications*, Royal Society of Chemistry, 2014.

9 S. Maiti, S. Banerjee and S. K. Palit, *Prog. Polym. Sci.*, 1993, **18**, 227–261.

10 Z. Tan, C. Wu, M. Zhang, W. Lv, J. Qiu and C. Liu, *RSC Adv.*, 2014, **4**, 41705–41713.

11 M. M. Alam, B. Biswas, A. K. Nedeltchev, H. Han, A. D. Ranasinghe, P. K. Bhowmik and K. Goswami, *Polymers*, 2019, **11**, 1141.

12 E. D. Weil and S. V. Levchik, *Phosphorus-Containing Polymers and Oligomers, Encyclopedia of Polymer Science and Technology*, John Wiley & Sons, 2010.

13 F. R. Wurm, *Green Mater.*, 2016, **4**, 135–139.

14 S. Iliescu, G. Ilia, A. Pascariu, A. Popa and N. Plesu, *Pure Appl. Chem.*, 2007, **79**, 1879–1884.

15 T. A. DelDonno, *US Pat.*, 5191029, Washington, DC: U.S. Patent and Trademark Office, 2013.

16 S. Monge, B. Canniccioni, A. Graillot and J. J. Robin, *J. Biol. Macromol.*, 2011, **12**, 1973–1982.

17 S. Iliescu and G. Ilia, *Curr. Green Chem.*, 2014, **1**, 40–50.

18 K. Dück, B. W. Rawe, M. R. Scott and D. P. Gates, *Angew. Chem., Int. Ed.*, 2017, **56**, 9507–9511.

19 S. Hiranphinyophat and Y. Iwasaki, *Sci. Technol. Adv. Mater.*, 2021, **22**, 301–316.

20 A. E. M. Hussein, W. M. Youssef, M. H. Taha and M. M. El-Maadawy, *Arab J. Nucl. Sci. Appl.*, 2017, **50**, 156–170.

21 A. E. M. Hussein, W. M. Youssef and A. S. El-Sheikh, *Radiochemistry*, 2019, **61**, 592–597.

22 W. M. Youssef, *J. Basic Environ. Sci.*, 2020, **7**, 1–12.

23 M. H. Taha, M. M. El-Maadawy, A. E. M. Hussein and W. M. Youssef, *J. Radioanal. Nucl. Chem.*, 2018, **317**, 685–699.

24 M. M. Shehata, W. M. Youssef, H. H. Mahmoud and A. M. Masoud, *Russ. J. Inorg. Chem.*, 2020, **65**, 279–289.

25 W. M. Youssef, A. S. El Sheikh, S. H. Ahmed and A. M. A. Morsy, *J.Radioanal. Nucl. Chem.*, 2020, **324**, 87–96.

26 A. A. Abdel-Samad, M. M. Abdel Aal, E. A. Haggag, W. M. Yosef and J. Bas, *Environ. Sci.*, 2020, **7**, 140–153.

27 W. M. Youssef, *Int. J. Environ. Anal. Chem.*, 2022, **1–20**, DOI: 10.1080/03067319.2022.2134995.

28 Z. Marczenko, *Spectrophotometric Determination of Elements*, E. Horwood, Halsted Press, Chichester, Eng., New York, 1976, p. 580.

29 L. Guo, B. Zhang, S. Bai, X. Ma and Z. Wang, *e-Polymers*, 2015, **15**, 195–201.

30 G. Socrates, *Infrared and Raman Characteristic Group Frequencies: Tables and Charts*, John Wiley & Sons Ltd, New York, 3rd edn, 2004.

31 Z. Moldovan, F. Ionescu, I. Vasilescu, S. LiŃescu and G. L. Radu, *An. Univ. Bucuresti, Chim.*, 2007, 49–57.

32 U. Shoukat, E. Baumeister and H. K. Knuutila, *Energies*, 2019, **12**, 3285.

33 M. Hema, S. Selvasekarapandian, D. Arunkumar, A. Sakunthala and H. Nithya, *J. Non-Cryst. Solids*, 2009, **355**, 84–90.

34 O. S. Amuda, A. Giwa and I. A. Bello, *Eng. J.*, 2007, **36**, 174–181.

35 C. Kütahyalı and M. Eral, *Sep. Purif. Technol.*, 2004, **40**, 109–114.

36 L. Xia, K. Tan, X. Wang, W. Zheng, W. Liu and C. Deng, *J. Environ. Chem. Eng.*, 2013, **139**, 887–895.

37 J. Wang and X. Guo, *J. Hazard. Mater.*, 2020, **390**, 122156.

38 X. Fan, L. Peng, X. Wang, S. Han, L. Yang, H. Wang and C. Hao, *Ind. Crops Prod.*, 2022, **183**, 114966.

39 A. Bhatnagar and A. K. Jain, *J. Colloid Interface Sci.*, 2005, **281**, 49–55.

40 F. A. Al-Rub, M. Kandah and N. Al-Dabaybeh, *Eng. Life Sci.*, 2002, **2**, 111–116.

41 J. Perić, M. Trgo and N. V. Medvidović, *Water Res.*, 2004, **38**, 1893–1899.

42 L. Zhong, F. He, Z. Liu, B. Dong and J. Ding, *Colloids Surf., A*, 2022, **641**, 128565.

43 M. Zhao, Z. Cui, D. Pan, F. Fan, J. Tang, Y. Hu and W. Wu, *ACS Appl. Mater. Interfaces*, 2021, **13**, 17931–17939.

44 Z. Xiao-teng, J. Dong-mei, X. Yi-qun, C. Jun-chang, H. Shuai and X. Liang-shu, *J. Chem.*, 2019, **1**, 6409504.

45 D. Mei, L. Liu and B. Yan, *Coord. Chem. Rev.*, 2023, **475**, 214917.

46 W. M. Youssef, M. S. Hagag and A. H. Ali, *Adsorpt. Sci. Technol.*, 2018, **36**, 1274–1293.

47 M. M. El-Maadawy, *Radiochemistry*, 2019, **61**, 331–338.

48 A. M. Masoud, M. Saeed, M. H. Taha and M. M. El-Maadawy, *J. Chem.*, 2020, **63**, 721–741.

49 C. Pang, Y. Liu, X. Cao, R. Hua, C. Wang and C. Li, *J. Radioanal. Nucl. Chem.*, 2010, **286**, 185–193.

50 W. M. Youssef, A. A. Elzoghby, A. A. Rateb, E. M. Helmy, K. A. Khalil and H. S. Gado, *Radiochemistry*, 2024, **66**, 481–492.